

# Toward an ideal integrating nephelometer

Ravi Varma,\* Hans Moosmüller, and W. Patrick Arnott

*Desert Research Institute, University of Nevada System, 2215 Raggio Parkway, Reno, Nevada 89512*

Received December 4, 2002

The Integrating Sphere Integrating Nephelometer is a novel and unique reciprocal nephelometer that uses an integrating sphere with attached truncation-reduction tubes to contain the sample volume and to integrate the scattered light. Its main advantage compared with current integrating nephelometers is a sevenfold reduction in truncation angle, which reduces errors in measured scattering from large particles. Additional features include improved sampling efficiency for large particles and a well-defined operating wavelength.

© 2003 Optical Society of America

OCIS codes: 120.5820, 010.1310.

Scattering of light by atmospheric aerosols in the visible and near-visible spectral regions influences the Earth's climate by changing short-wave radiative forcing<sup>1,2</sup> and influences optical remote sensing by ground-based, airborne, and satellite systems,<sup>3</sup> including visual perception by human beings.<sup>4</sup> The contribution of suspended particles to atmospheric scattering is highly variable in space and time and generally dominates the total extinction in the visible near the Earth's surface.

Particle scattering is commonly characterized by integrating nephelometers that measure the scattering component of extinction, also known as the total scattering coefficient. The necessary integration of the scattered light over all angles (i.e.,  $4\pi$ ) is performed geometrically with one of two schemes devised by Beuttell.<sup>5,6</sup> Either a cosine-law diffuse light source is used to illuminate the scattering volume that is viewed with a detector; or detector and light source are reversed, a parallel light beam is used, and the scattered light is detected by a cosine detector. The first arrangement is more common,<sup>7-9</sup> and the second arrangement is known as a reciprocal nephelometer.<sup>10-12</sup>

An ideal integrating nephelometer provides a direct measurement of the total scattering coefficient of suspended particles independently of their properties such as size, composition, and physical state.<sup>9</sup> Real integrating nephelometers fall short of this ideal, mostly because of imperfect angular and wavelength response and imperfect particle sampling.

Imperfect angular response arises because illumination intensity or detector sensitivity should be cosine weighted but is not. In particular, light scattered at angles smaller than  $\sim 7^\circ$  and larger than  $\sim 170^\circ$  is not detected by modern integrating nephelometers.<sup>9</sup> These angles are known as truncation angles. As the angular distribution of particle scattering is strongly dependent on particle size, the scattering coefficient measured with an integrating nephelometer depends on the instrument's truncation angles. For large particles, at least half of the scattered light is due to near-forward diffraction, which may not be detected.<sup>13</sup> The resultant truncation error is the fraction of the total scattered power that is not detected because of angular truncation. Angularly resolved scattering measurements are also plagued by truncation errors, limiting their ability to measure asymmetry parameter  $g$ .<sup>14,15</sup>

Imperfect aerosol sampling results in an aerosol in the measurement volume that has different scattering properties from the ambient aerosol of interest. Sampling losses of large particles as a result of impaction and gravitational settling are common.

Imperfect wavelength response is due to the integration of particle scattering over a wavelength range that is typically 40 nm for commercial nephelometers that use a thermal light source and a bandpass filter.<sup>9</sup> As the wavelength dependence of particle scattering is size and refractive-index dependent, the measured scattering coefficient is appropriate not for the nominal wavelength but only for the system's spectral bandpass with appropriate weighting for the combined spectral response of light source, detector, filter, and other optical elements.<sup>16</sup> The Integrating Sphere Integrating Nephelometer (ISIN) described in what follows reduces all three imperfections.

The Desert Research Institute (DRI) ISIN is a unique reciprocal nephelometer that uses an integrating sphere with attached truncation-reduction tubes to contain the sample volume and to integrate the scattered light (Fig. 1). It improves on the imperfect angular response by reducing forward (backward) truncation angles to  $\approx 1^\circ$  ( $\approx 179^\circ$ ), it reduces sampling losses by employing a fairly straight vertical flow path, and it eliminates imperfect wavelength response by utilizing a narrowband laser as light source. A related design using a homogeneously illuminated integrating sphere containing the sample and a view path through the sphere into a light trap is the reciprocal of our basic design (minus truncation-reduction tubes),<sup>5,6</sup> but it does not reduce truncation angle and losses.

Refer to Fig. 1: A frequency-doubled, all-solid-state, continuous-wave Nd:YAG laser operating at 532 nm is used as a light source. Its chopped beam is spatially filtered to reduce wall scattering, and its power is monitored with a beam splitter and a photodiode attached to a small integrating sphere. The main beam enters the forward truncation-reduction tube through a window and propagates through the integrating sphere's entrance aperture, its center, its exit aperture, and the backward truncation-reduction tube into a beam trap.

The integrating sphere is machined from solid aluminum with diameter  $d_0 = 20$  cm and is segmented into two parts for easy access to its interior. Laser

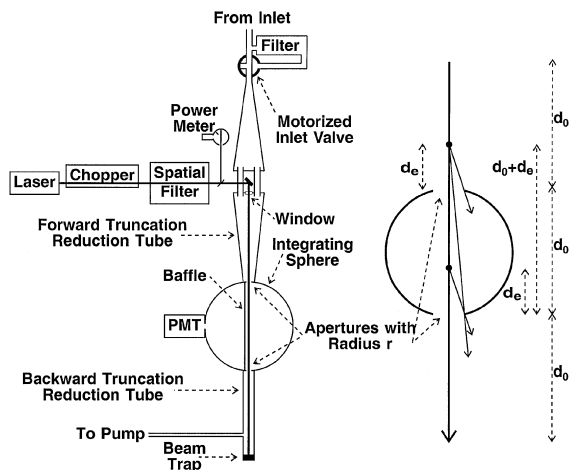


Fig. 1. Left, schematic diagram and right, forward-scattering truncation geometry of the DRI ISIN.

beam entrance and exit apertures of radius  $r$  ( $r = 5$  mm) are located on opposite poles of the sphere, and a truncation-reduction tube of length  $d_0$  is attached to each aperture (Fig. 1). A third aperture of identical size is located on the equator of the sphere with a photomultiplier tube (PMT) attached. The inside surface of the sphere is coated with a highly reflecting ( $>99\%$ ) and near-Lambertian barium sulfate-based coating. The insides of the truncation-reduction tubes are coated black to prevent reflection of scattered light. Laser light scattered by the medium in the sphere is integrated by multiple diffuse reflections in the sphere<sup>17,18</sup> and consequently measured by the PMT. A 20-cm-long, 1-cm-wide baffle, also coated white, is mounted parallel to the laser beam to prevent light scattered by the medium from directly reaching the PMT. The basic setup (minus truncation-reduction tubes) is similar to that used to measure the total scattering loss of optical fiber,<sup>19</sup> with the fiber replaced by the scattering medium. Although the total area of the integrating sphere ports (entrance + exit + PMT aperture =  $2.4$  cm<sup>2</sup>) is very small ( $<0.2\%$ ) compared with the total inside surface of the sphere ( $0.13$  m<sup>2</sup>), loss of scattered light through the exit aperture can be significant for large particles, which scatter predominantly in the near-forward direction.<sup>13</sup>

The following discussion centers on the primary innovation provided by the ISIN, the property of low truncation error. The DRI ISIN geometry is symmetric with respect to forward- and backward-scattering truncation errors. However, this discussion is limited to the more important forward truncation errors.<sup>13</sup> Therefore this discussion is limited to forward truncation errors. First, consider only an integrating sphere filled with the scattering medium and equipped with circular entrance and exit apertures of radius  $r$ . A laser beam propagates along the sphere axis and is scattered by the scattering medium. Forward truncation angle  $\alpha$  depends on distance  $d_e$  from the scattering location in the sphere to the exit aperture as  $\alpha_e = \tan^{-1}(r/d_e)$  and varies from  $1.4^\circ$  to  $90^\circ$  with an average of  $6.7^\circ$ . To better confine the angles of both forward and backward truncation we attach truncation-reduction tubes of length  $d_0$  to each

aperture and fill them with the scattering medium. Now, for each location in the sphere at a distance  $d_e$  from the exit aperture with a truncation angle  $\alpha(d_e) = \tan^{-1}(r/d_e)$ , there exists a location  $d_0 + d_e$  in the truncation-reduction tube at a distance  $d_e$  from the entrance aperture (Fig. 1). Light that has been near-forward scattered from location  $d_e$  in the sphere at angles smaller than  $\alpha(d_e)$  is still lost through its exit aperture. The same amount of light, however, is now near-forward scattered into the sphere at angles smaller than  $\alpha(d_e)$  through its entrance aperture from location  $d_0 + d_e$  in the forward truncation-reduction tube. This compensation is not complete, as the central portion of the light that is near-forward scattered into the sphere leaves the sphere through its exit aperture. This yields an effective truncation angle  $\alpha(d_e + d_0) = \tan^{-1}[r/(d_e + d_0)]$  that varies from  $0.7^\circ$  to  $1.4^\circ$ , with an average of  $1.0^\circ$ . Although longer truncation-reduction tubes or smaller apertures could further reduce the truncation angles, there is a trade-off with system size and flow properties.

For large particles the truncation error can be approximated by diffraction theory and scales with  $x \sin(\alpha)$  or for small truncation angles  $\alpha$  with  $x \alpha$ ,<sup>13</sup> where  $x$  is the size parameter, the ratio of particle circumference to wavelength. Therefore a reduction of the truncation angle from  $7^\circ$  to  $1^\circ$  permits detection of scattering from approximately seven-times-larger particles with identical truncation error. Forward truncation errors from Mie and diffraction theory are shown for nephelometers with  $7^\circ$  and  $1^\circ$  truncation angles as functions of particle diameter in Figs. 2(a) and 2(b) for absorbing and nonabsorbing particles, respectively. For absorbing particles diffraction accounts for most of the scattered light, whereas for nonabsorbing particles it accounts for half of the scattered light.<sup>13</sup> For example, truncation errors larger than 25% occur for nonabsorbing (absorbing) particles at diameters larger than  $\sim 16$   $\mu\text{m}$  ( $11$   $\mu\text{m}$ ) for a truncation angle of  $1^\circ$  and at diameters larger than  $\sim 2.3$   $\mu\text{m}$  ( $1.4$   $\mu\text{m}$ ) for a truncation angle of  $7^\circ$ . Strongly absorbing particles in the atmosphere are mostly black carbon combustion products with submicrometer particle diameters, which do not contribute much to truncation errors. Exceptions are large iron-bearing mineral dust particles, which can have substantial optical absorption, thereby increasing truncation errors. For nonabsorbing particles, a nephelometer with a truncation angle of  $7^\circ$  loses a substantial part (i.e.,  $>25\%$  at  $d > 2.3$   $\mu\text{m}$ ) of scattering from the coarse particle mode, whereas the DRI ISIN with a truncation angle of  $1^\circ$  measures nearly all scattering from atmospheric aerosol. The 25% cutoff for the DRI ISIN occurs at  $16$   $\mu\text{m}$ , where the gravitational settling velocity ( $\approx 0.8$  cm/s for a density of  $\approx 1$  g/cm<sup>3</sup>) is nearly a factor of 50 [ $\approx (16/2.3)^2$ ] larger than at  $2.3$   $\mu\text{m}$  and where most particles are removed from the atmosphere in a matter of hours.<sup>20</sup>

The light scattered in the integrating sphere is detected with a PMT, and its signal and the signal from the photodiode monitoring the laser power are measured with phase-sensitive detection (implemented in software) at the chopping frequency. The PMT

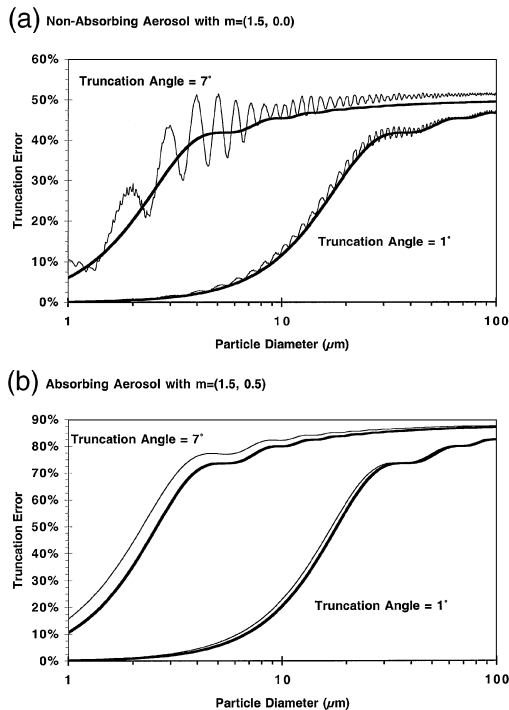


Fig. 2. Truncation errors for (a) nonabsorbing aerosol and (b) absorbing aerosol (thinner curves, Mie theory; thicker curves, diffraction theory).

signal is normalized to the laser power and converted into a scattering coefficient after instrument calibration. Ancillary data acquired include time, temperature, pressure, and relative humidity.

Inlet air is sampled from the top through a vertical 1.3-cm I.D. stainless-steel tube that can alternate under computer control between unfiltered and HEPA filtered (Fig. 1). The inlet tube expands conically and is split into four individual 1.3-cm I.D. tubes, which reunite and narrow after coupling the laser beam into the center of the flow. The flow enters and exits the integrating sphere through its 1-cm-diameter apertures and terminates in the flow pump. The vertical flow arrangement minimizes losses caused by gravitational settling and nonisokinetic sampling. At a flow rate of 15 L/min, these sampling losses are estimated to be ~13% (~30%) for 10- $\mu$ m- (16- $\mu$ m-) diameter particles. The Reynolds number is below the turbulence threshold at all junctions and inlets.

The DRI ISIN has been calibrated with two independent, primary calibration schemes: (a) the common method of calibrating nephelometers with two gases with different and well-known scattering coefficients ( $\text{CO}_2$  and HEPA-filtered air<sup>9,21</sup>) and (b) introduction of a plate with well-known diffuse reflectivity  $R_C$  blocking the exit aperture of the integrating sphere in conjunction with a reduction in laser power by a neutral-density filter with optical density OD. The measured signal in the latter case corresponds to a scattering coefficient of  $10^{-\text{OD}}R_C/d_0$ . Results from both calibration schemes agreed within the measurement error. Initial comparisons of the DRI ISIN with two other nephelometers (TSI, Inc., 3563 and Radiance Research M903) with submicrometer particles revealed excellent correlation and agreement within

a few percent. Comparisons with the M903 nephelometer during a study of dust entrainment showed good agreement for ambient fine particles, whereas the DRI ISIN readings were as much as four-times higher than those of the M903 for freshly entrained coarse particulate matter. This large discrepancy is attributed to the improved angular response, including a reduction of the truncation error by as much as a factor of 2, and to the improved large particle sampling of the DRI ISIN compared to the M903.

This research was supported in part by grants from the National Science Foundation (ATM-9871192), the U.S. Department of Defense (SERDP CP-1191), and the U.S. Department of Energy Pacific Northwest National Laboratory (3492), and by the Applied Research Initiative of the State of Nevada. It is a pleasure to acknowledge C. F. Rogers's contributions to the sampling design of the DRI ISIN. H. Moosmüller's e-mail address is hansm@dri.edu.

\*Present address, Arcadis, Inc., P.O. Box 13109, Research Triangle Park, North Carolina 27709.

## References

1. A. K. Jain, B. P. Briegleb, K. Minschwaner, and D. J. Wuebbles, *J. Geophys. Res.* **105**, 20773 (2000).
2. M. S. Reddy and C. Venkataraman, *Atmos. Environ.* **34**, 4511 (2000).
3. J. R. Schott, *Remote Sensing: The Image Chain Approach* (Oxford U. Press, New York, 1997).
4. J. G. Watson, *J. Air Waste Manage. Assoc.* **52**, 626 (2002).
5. R. G. Beuttell and A. W. Brewer, *J. Sci. Instrum.* **26**, 357 (1949).
6. J. Heintzenberg and R. J. Charlson, *J. Atmos. Ocean. Technol.* **13**, 987 (1996).
7. N. C. Ahlquist and R. J. Charlson, *J. Air Pollut. Control Assoc.* **17**, 467 (1967).
8. R. J. Charlson, *Atmos. Tech.* **12**, 10 (1980).
9. T. L. Anderson, D. S. Covert, S. F. Marshall, M. L. Laucks, R. J. Charlson, A. P. Waggoner, J. A. Ogren, R. Caldwell, R. L. Holm, F. R. Quant, G. J. Sem, A. Wiedensohler, N. A. Ahlquist, and T. S. Bates, *J. Atmos. Ocean. Technol.* **13**, 967 (1996).
10. H. E. Gerber, *Appl. Opt.* **18**, 1009 (1979).
11. G. W. Mulholland and N. P. Bryner, *Atmos. Environ.* **28**, 873 (1994).
12. M. A. Peñaloza M., *Meas. Sci. Technol.* **10**, R1 (1999).
13. H. Moosmüller and W. P. Arnott, "Angular truncation errors in integrating nephelometry," *Rev. Sci. Instrum.* (to be published).
14. P. N. Francis, *J. Atmos. Sci.* **52**, 1142 (1995).
15. H. Gerber, Y. Takano, T. J. Garrett, and P. V. Hobbs, *J. Atmos. Sci.* **57**, 3021 (2000).
16. J. M. Rosen, R. G. Pinnick, and D. M. Garvey, *Appl. Opt.* **36**, 2642 (1997).
17. R. Ulbricht, *Elektrotech. Z.* **21**, 595 (1900).
18. J. A. Jacquez and H. F. Kuppenheim, *J. Opt. Soc. Am.* **45**, 460 (1955).
19. Labsphere, Inc., *A Guide to Integrating Sphere Photometry and Radiometry* (Labsphere, North Sutton, N.H., 1994).
20. W. C. Hinds, *Aerosol Technology*, 2nd ed. (Wiley Interscience, New York, 1999).
21. H. Horvath and W. Kaller, *Atmos. Environ.* **28**, 1219 (1994).